Ocean Engineering 266 (2022) 113054

Contents lists available at ScienceDirect

Ocean Engineering

journal homepage: www.elsevier.com/locate/oceaneng

Short communication

LQ optimal robust multivariable PID control for dynamic positioning of ships with norm-bounded parametric uncertainties

Falguni Gopmandal *, Arun Ghosh, Avinash Kumar

Department of Electrical Engineering, IIT Kharagpur, West Bengal, Kharagpur 721302, India

ARTICLE INFO

Keywords:
Dynamic positioning
MIMO PID control
Norm-bounded uncertainty
Robust LQ performance

ABSTRACT

The design of a suitable controller for dynamic positioning (DP) of ships is a challenging task keeping the hydrodynamic uncertainties in mind. The magnitude and rate constraints on the actuators make the problem more difficult. The present work employs a two-degree-of-freedom (2-DOF), multivariable, proportional–integral–derivative (PID) control for DP of a ship. To design the controller, first, the ship dynamics with hydrodynamic parameter uncertainties is represented in an uncertain state-space descriptor form. Then, the design of feedback gains of 2-DOF PID controller for the uncertain descriptor plant is converted into a state feedback design for an augmented uncertain descriptor plant. Next, a linear matrix inequality-based condition is obtained to solve this state feedback problem in order to ensure a desired linear quadratic (LQ) performance, even in presence of uncertainties. Finally, to further improve the tracking performance, the feedforward gain of the 2-DOF PID controller is designed using $\mathcal{H}_\infty$ approach. The DP performance of the proposed controller is tested for the considered ship model along with uncertainties, actuator constraints, and environmental disturbances. A comparison with the existing PID controllers is also carried out to show superiority of the proposed controller.

1. Introduction

Control systems for station keeping and low-speed maneuvering of ships are commonly known as dynamic positioning (DP) systems. The presence of environmental disturbances, such as wind, waves, ocean currents, and uncertainties in hydrodynamic mass and damping matrices of the ship make the control design for DP system really challenging. Additionally, the constraints on magnitude and rate of the control deflections make the design more complicated.

Several advanced techniques on designing controllers for DP systems are reported in literature. $\mathcal{H}_\infty$ controllers are used for DP application in Katebi et al. (1997), You et al. (2017), and Hassani et al. (2017). In Katebi et al. (1997), You et al. (2017), the robustness as well as regulation of environmental disturbances are taken care of by imposing $\mathcal{H}_\infty$ constraints in the design. To achieve desired performance even in presence of uncertainties, which amounts to robust performance, a mixed μ synthesis approach is used to design $\mathcal{H}_\infty$ controllers in Hassani et al. (2017). As linear controllers additionally need gain-scheduling to control a nonlinear system like ship over wide range of operating conditions, nonlinear controllers are also employed for DP systems. The nonlinear schemes widely used for the DP system, are mostly based on (i) backstepping (Fossen and Berge, 1997; Fossen and Grovlen, 1998; Yu et al., 2018; Witkowska and Śmierzchalski, 2018), (ii) sliding mode (Tannuri et al., 2010; Liang et al., 2020), (iii) adaptive (Hu et al., 2017; Li et al., 2020; Lu et al., 2021; Huang et al., 2021; Du et al., 2015; Cui et al., 2021; Yu et al., 2018; Lin et al., 2018; Hu et al., 2015; Wang et al., 2021; Witkowska and Śmierzchalski, 2018; Liang et al., 2020; Wang et al., 2019), (iv) fuzzy logic (Lin et al., 2018; Hu et al., 2015; Wang et al., 2021; Chang et al., 2002; Zhang et al., 2021; Wang et al., 2019; Xu et al., 2020), (v) neural network (Zhang et al., 2016, 2020), and (vi) model predictive controls (Zheng et al., 2020; Veksler et al., 2016; Jayasiri et al., 2017). In many cases, hybrid of two or more of these schemes (Liang et al., 2020; Lin et al., 2018; Hu et al., 2015; Wang et al., 2021; Yu et al., 2018; Witkowska and Śmierzchalski, 2018; Wang et al., 2019) are used for better performance. The output feedback backstepping controllers are observer-based, and Lyapunov method is used for globally exponentially stability analysis. The sliding mode controllers are suitable to make the system robust against matched uncertainties and disturbances, but special care needs to be taken to avoid chattering. The observer-based robust adaptive controllers are suitable for systems with parametric uncertainties, but the closed-loop

* Corresponding author.
E-mail address: falgun.ece@gmail.com (F. Gopmandal).

https://doi.org/10.1016/j.oceaneng.2022.113054
Received 31 May 2022; Received in revised form 15 October 2022; Accepted 28 October 2022
Available online 17 November 2022

stability cannot be guaranteed in presence of time-varying environmental disturbances. While all these controllers need explicit model of the plant, fuzzy logic and neural network-based controllers do not, but the stability robustness in presence of uncertainties and disturbances is difficult to guarantee. Nonlinear model predictive control, on the other hand, is well known to explicitly handle state and control input constraints in the DP system. In summary, the order of the existing $\mathcal{H}_\infty$ controllers is the plant order plus the order of the weights, which naturally becomes high. As a result, their practical implementation becomes difficult. The order of the nonlinear controllers also becomes high because of the use of state observers to implement the control laws. Further, the stability analysis becomes extremely complex with the nonlinear controllers, in particular, with time-varying disturbances and uncertainties. Moreover, with the existing nonlinear controllers (e.g. disturbance observer-based nonlinear control) a desired performance was achieved in presence of disturbances, but it is not clear how to guarantee a desired performance even in presence parametric uncertainties, i.e., robust performance.

In view of the above study, for DP system, it is necessary to design low order, linear controllers, which can guarantee robust performance. As is well known, PID controllers are of low order, easy to implement in both analogue and digital fashions, and therefore, widely used in industries. The PID controller proposed in Balchen et al. (1980) for DP systems, however, needs Kalman filter-based state observer. To do away with observer, a multi-input multi-output (MIMO) or cross-coupled PID controller is proposed in Martin and Katebi (2005) for ship positioning control. Therein, the design is, however, based on transfer function method and the performance of this controller is heavily dependent on the suitable choice of bandwidth. A decentralized or multi-loop PID controller is used for the ship positioning system in Du et al. (2016) for comparison purpose. But, therein, the performance is not studied in presence of wave frequency disturbances which are unavoidable in ship positioning system. Actuator constraints are also not considered therein. Some fuzzy logic-based PID controllers are also reported for DP systems (Xu et al., 2020; Wang et al., 2019), but these controllers need state observer and moreover, stability robustness cannot be guaranteed with such controllers, as already mentioned towards the end of second paragraph above. Recently, in Soman et al. (2018), a state-space-based method for designing MIMO PID control for DP system is proposed to ensure optimal linear quadratic (LQ) performance for the nominal system. The main limitation of this design is that the system response deviates widely from the nominal one if uncertainties are present. This motivates one to propose a method for designing PID controller for DP system such that its response remains close to the nominal one even in presence of some uncertainties in the system parameters.

This paper proposes a state-space-based method to design a two-degree-of-freedom (2-DOF) multivariable PID controller in order to achieve desired LQ performance in presence of norm-bounded uncertainties in the hydrodynamic parameters of a ship DP system. To handle the above norm-bounded uncertainties, first, the uncertain ship dynamics is represented in a descriptor-based state-space form as in Lin et al. (2000). Next, to design the proposed MIMO PID controller, the PID design problem is converted into a state feedback control problem for an augmented uncertain descriptor system. Finally, the state feedback gains are computed using linear matrix inequality (LMI)-based method so as to achieve robust LQ performance. For designing the state feedback gains, the LMIs are derived following the $\mathcal{H}_\infty$ results of Lin et al. (2000) and Ren and Zhang (2010). (In this context, it is noteworthy that if one uses the weighted $\mathcal{H}_\infty$ cost as in Ren and Zhang (2010), then the PID design problem cannot be transformed into a direct state feedback control problem.) To enhance the tracking performance, the feedforward gain of the 2-DOF PID controller is designed via $\mathcal{H}_\infty$ method. The performance of the proposed PID scheme is compared with the existing PIDs in presence of hydrodynamic parameter uncertainties and disturbances during station keeping as well as low speed maneuvering.

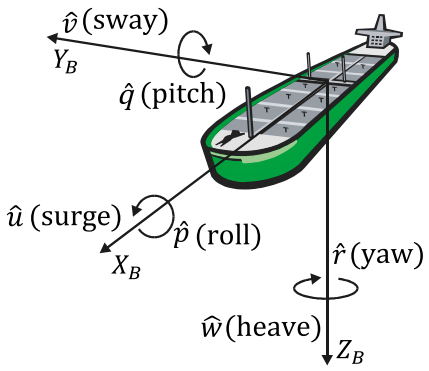

Fig. 1. 6-DOF motion of a vessel (Alme, 2008).

It may be noted that, PID controllers are also designed for norm-bounded uncertain systems in literature (Lin et al., 2004; Pradhan and Ghosh, 2022). In Lin et al. (2004), although a descriptor-based approach is used, the same is applicable to systems with full column rank output matrix only, which is very rare in practice. The method recently proposed in Pradhan and Ghosh (2022) is not applicable to descriptor systems.

The rest of the paper is organized as follows. In Section 2, the model of a surface vessel including high and low frequency disturbances that generally occur is described. The proposed multivariable 2-DOF PID control scheme and its LMI-based design methodology for robust LQ performance control of the DP system are presented in Section 3. The simulation and comparison results are presented in Section 4. Finally, the conclusion is drawn in Section 5.

Notations: In this paper, the symbol '*' is used to represent transpose of the off-diagonal block of a matrix in LMI. For a matrix X, say, $X + X^T$ is denoted by $\mathrm{Sym}(X)$. $\|T\|_\infty$ is the ∞-norm of a stable transfer function $T(s)$, i.e., $\|T\|_\infty := \sup_{\omega \geq 0} \sigma_{max}(T(j\omega))$ where $\sigma_{max}(.)$ denotes the maximum singular value. For a signal $x(t)$, $\|x\|_2$ stands for 2-norm of $x(t)$, i.e., $\|x\|_2 := \sqrt{\int_0^\infty x^T(t)x(t)dt}$. For a matrix X, $X > 0$ (< 0) implies, X is positive definite (or negative definite, respectively).

2. Mathematical modeling

In this section, the mathematical model of the system to be used is presented.

2.1. Ship model for DP

The 6-DOF of motion of a vessel is shown in Fig. 1. For DP, a 3-DOF of horizontal motion is obtained under some standard assumptions, such as (i) port-starboard symmetry, (ii) small pitch angle ($\phi \approx 0$), small roll angle ($\theta \approx 0$), (iii) surface vessel, and (iv) low speed (<2–3 m/s) maneuvering (Alme, 2008; Fossen, 2011) (Ch. 7). Under these assumptions, the 6-DOF model of the vessel can be simplified to the low-speed 3-DOF mass–spring–damper like model (Hassani et al., 2017; Alme, 2008; Loueipour et al., 2015) for DP, as given by

$$\begin{aligned} \dot{\eta} &= R(\psi)\upsilon \\ M\dot{\upsilon} + D\upsilon &= \tau + R^T(\psi)w_d \\ y_s &= \eta + v_d. \end{aligned} \tag{1}$$

Here, $\eta = [x, y, \psi]^T$ represents the position vector in Earth-fixed frame, where x is motion in the x-direction (surge), y is motion in the y-direction (sway), ψ is rotation about the z-axis (yaw or heading angle). The vector $\upsilon = [\hat{u}, \hat{v}, \hat{r}]^T$ represents velocity in body-fixed frame, where $\hat{u}$ is linear velocity in x-direction, $\hat{v}$ is linear velocity in y-direction, $\hat{r}$ is angular velocity about the z-axis. $\tau \in \mathbb{R}^3$ is the vector of control forces/torques produced by different propulsion devices. All these

propulsion devices will be referred as actuator in this work. $y_s \in \mathbb{R}^3$ is the sensor output. $w_d \in \mathbb{R}^3$, $v_d \in \mathbb{R}^3$ are the low and high frequency disturbances acting on the vessel in Earth-fixed frame. w_d occurs mainly due to wind and ocean current, and v_d due to the high frequency wave motion in position measurements (see Section 2.3 for details). In (1), $M = M_{RB} + M_A$ represents the mass matrix where, M_{RB} is rigid body mass matrix and M_A is hydro-dynamical added mass matrix due to the added mass of surrounding fluid and are given by

$$M_{RB} = \begin{bmatrix} m & 0 & 0 \\ 0 & m & mx_g \\ 0 & mx_g & I_z \end{bmatrix}, \; M_A = \begin{bmatrix} -X_{\dot{u}} & 0 & 0 \\ 0 & -Y_{\dot{v}} & -Y_{\dot{r}} \\ 0 & -N_{\dot{v}} & -N_{\dot{r}} \end{bmatrix}. \tag{2}$$

The rotational matrix $R(\psi)$ (which relates the body-fixed and Earth-fixed reference frames) and the hydro-dynamical damping matrix (D) are given by

$$R(\psi) = \begin{bmatrix} \cos(\psi) & -\sin(\psi) & 0 \\ \sin(\psi) & \cos(\psi) & 0 \\ 0 & 0 & 1 \end{bmatrix}, D = \begin{bmatrix} -X_u & 0 & 0 \\ 0 & -Y_v & mu_0 - Y_r \\ 0 & -N_v & mx_g u_0 - N_r \end{bmatrix}$$

where the cruise speed (i.e., horizontal velocity) $u_0 = \sqrt{\hat{u}_0^2 + \hat{v}_0^2} = 0$ for station keeping and $u_0 > 0$ for low speed maneuvering (Fossen and Berge, 1997; Fossen and Strand, 1999). Further, with the assumptions (i), (iv), as mentioned at the beginning of this paragraph, $N_{\dot{v}} = Y_{\dot{r}}$, implying $M = M^T > 0$ (Fossen and Berge, 1997; Fossen and Strand, 1999). Note, the block-diagonal structure of M, D implies that the surge motion is decoupled from sway and yaw motions.

2.2. Actuator model

As assumed in von Ellenrieder (2019) and Fossen and Berge (1997), in this paper, we consider the actuator dynamics as

$$T_a \dot{\bar{u}} + \bar{u} = u_c \tag{3}$$

where $\bar{u} \in \mathbb{R}^q$ is the vector of actuator states, $u_c \in \mathbb{R}^q$ is the vector of control inputs, $T_a \in \mathbb{R}^{q \times q}$ is the diagonal matrix of actuator time constants. The actuator state $\bar{u}$ is related to τ in (1) by

$$\tau = B_{\bar{u}} \bar{u} \tag{4}$$

where $B_{\bar{u}} \in \mathbb{R}^{3 \times q}$ is the actuator configuration matrix.

2.3. Disturbance model

As mentioned in Katebi et al. (1997, 2001), the frequency content of environmental disturbances in a DP system can be approximately decoupled into low frequency and high frequency components. The second order sea wave, turbulent wind, and measurement noise are regarded as high frequency ($\omega > 0.7$ rad/s) disturbances, whereas the ocean current and constant wind as low frequency ($\omega < 0.5$ rad/s) disturbances. The low frequency disturbance causes undesired drift of the vehicle and therefore the controller is required to compensate for the same using the thrusters. The high frequency disturbances cause unnecessary oscillatory motion in the ship and therefore they are attenuated in the loop using suitable notch filters to avoid wear and tear of thrusters.

2.3.1. Low frequency (LF) disturbance model

The LF disturbances in surge, sway, and yaw channels can be assumed to be decoupled from each other. The first order transfer function (Katebi et al., 1997) used to represent the frequency response of the LF disturbance model for each channel is given by

$$R_{l_i}(s) = \frac{c_{1_i} s + c_{2_i}}{d_i s + 1} \tag{5}$$

where $i = 1, 2, 3$ denote the surge, sway, and yaw channels, respectively. Then, the LF disturbance vector $w_d(t)$ is represented by $w_d(s) = \text{diag}\{R_{l_i}(s)\}\xi_l(s)$, where, $\xi_l(t)$ is a vector of white noises with unit variance and zero mean. In the present work, we consider $c_{1_i} = 0$, $c_{2_i} = d_i = 100$ (Katebi et al., 1997). With these parameters, the frequency response of $R_{l_i}(s)$ is as shown in Fig. 2. It shows that the bandwidth of w_d(t) is $1/d_i = 0.01$ rad/s and has a mean magnitude of $c_{2_i} = 100$ (i.e., 40 dB). The high gain of $R_{l_i}(s)$ at LF implies that the control loop gain at LF should be high, so that the effect of LF disturbance gets attenuated at the output.

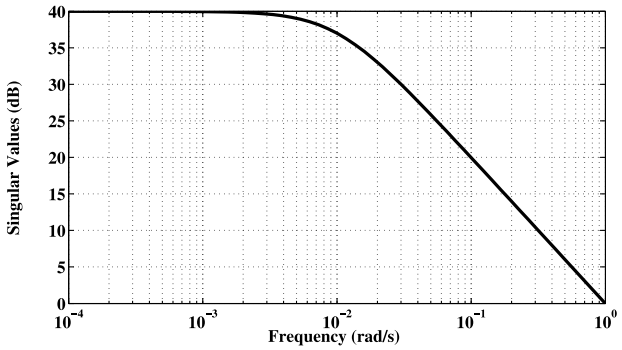

Fig. 2. Frequency response of LF disturbance model.

2.3.2. High frequency (HF) disturbance model

The HF or wave frequency (WF) disturbance model for each channel is considered as

$$R_{h_i}(s) = \frac{a_i s^2 + 2\zeta_{1_i}\omega_{h_i} s + \omega_i^2}{b_{h_i}(s^2 + 2\zeta_{2_i}\omega_{h_i} s + \omega_{h_i}^2)} \tag{6}$$

where $i = 1, 2, 3$ denote the surge, sway and yaw channels, respectively (Katebi et al., 1997). The HF disturbance vector $v_d(t)$ is represented by $v_d(s) = \text{diag}\{R_{h_i}(s)\}\xi_h(s)$, where, $\xi_h(t)$ is a vector of white noises with unit variance and zero mean. In this work, we choose $b_{h_i} = \omega_{h_i} = 1$, $\zeta_{2_i} = 0.065$, $a_1 = 2$, $\zeta_{1_1} = 8$, $\omega_1 = 0.141$, $a_2 = 1.5$, $\xi_{1_2} = 6$, $\omega_2 = 0.122$, $a_3 = 1$, $\zeta_{1_3} = 4$, $\omega_3 = 0.1$ (Katebi et al., 1997). With these parameters, the frequency response of $R_{h_i}(s)$ is as shown in Fig. 3. It shows that for all three channels, the resulting $v_d(t)$ has peak frequency of $\omega_{h_i} = 1$ rad/s. It can also be seen that $v_d(t)$ has maximum average magnitudes of ζ_{1_i}/ζ_{2_i}, i.e., 123.07, 92.3, 61.53, in surge, sway, and yaw channels, respectively. The mean magnitude of $v_d(t)$ in the low frequency band is $\omega_i^2/(b_{h_i}\omega_{h_i}^2)$ which is very small (within -30 to -40 dB). This implies that the HF disturbance has very small effect in the LF range. The HF steady-state gain of $R_{h_i}(s)$ is a_i/b_{h_i}, i.e., 2, 1.5, and 1 in surge, sway, and yaw channels, respectively. This implies, the surge and sway channels are more sensitive to HF measurement noise, and the control loop gain at HF should be sufficiently small to attenuate these. As $\omega_{h_i} = 1$ rad/s, the range of frequencies over which the attenuation of the WF disturbances needed using suitable wave filtering is around 0.1 rad/s to 10 rad/s. Beyond 10 rad/s, the disturbances (i.e., measurement noise) are attenuated by low control loop gain at HF.

3. Ship positioning control system

The feedback configuration for DP of a ship is shown in Fig. 4, where $y = \eta$ and $r = [x_r, y_r, \psi_r]^T$ is the reference input vector for low speed maneuvering. The details of ship dynamics, actuator dynamics, disturbance models are already discussed in Section 2. Here, the controller (the details of which are provided in Section 3.3) is used to attenuate the effect of LF disturbance (w_d), such as constant wind, wave and sea currents, and to achieve low speed maneuvering. The wave filter (see Section 3.5) in the feedback loop helps reject the WF disturbances v_d. Thus, the presence of wave filter helps prevent undesired modulation of thrusters due to WF disturbances.

In this paper, the actuator dynamics is neglected during controller design as it is much faster than the ship dynamics. However, the

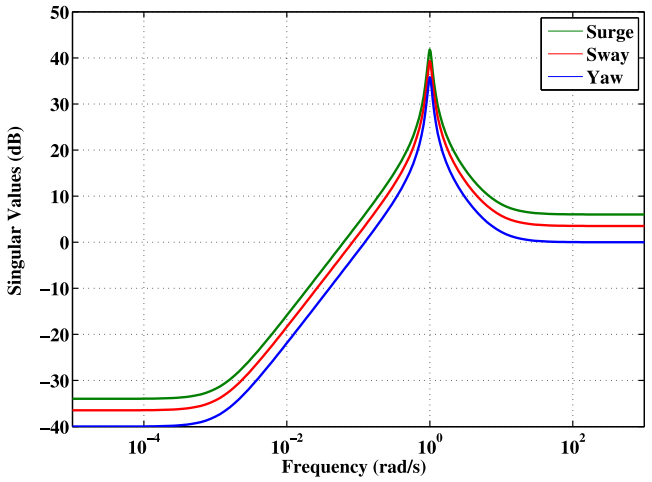

Fig. 3. Frequency response of HF disturbance model.

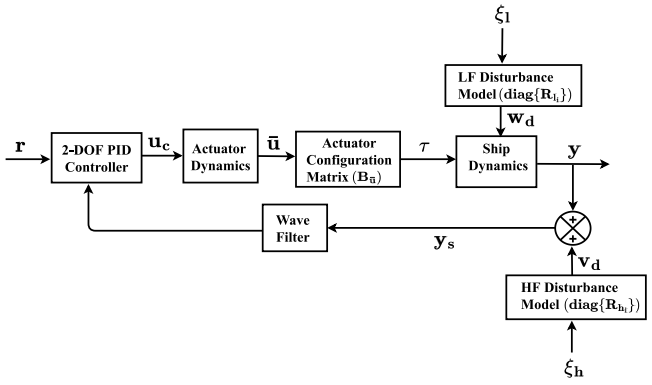

Fig. 4. Block diagram for ship positioning control system.

performance and robustness of the compensated system are studied after including the actuator dynamics. Now, if in (4), $q \geq 3$, one can write $\bar{u} = B_{\bar{u}}^T(B_{\bar{u}}B_{\bar{u}}^T)^{-1}\tau$. Further if the actuator dynamics (3) is neglected, then $u_c = \bar{u}$, signifying

$$u_c = B_{\bar{u}}^T(B_{\bar{u}}B_{\bar{u}}^T)^{-1}\tau. \tag{7}$$

This means that for designing the controller, one can consider the dynamics given by (1) as a plant with $\tau = u$ as the control input. Then the actual control input (i.e., input to the actuators) becomes (7). The same will be followed in this paper.

3.1. State-space description of the plant in descriptor form

The presence of rotational matrix $R(\psi)$ makes the system (1) nonlinear. In this paper, for controller design, we linearize this nonlinear system around an operating point origin (i.e., $\psi = 0$) (Fossen, 2011) (Chapter 7). Then, the linearized model of the ship DP system becomes

$$\begin{aligned}\dot{\eta} &= \upsilon\\ M\dot{\upsilon} + D\upsilon &= \tau\\ y &= \eta.\end{aligned} \tag{8}$$

Note, in above, the disturbances w_d, v_d are not considered because, the main objective of the present work is to guarantee robust LQ performance, where exogenous signals are discarded. However, as these disturbances are unavoidable, later on, the performance of the controller is studied in presence of the same. As is well known, an LQ performance control has good LF input disturbance attenuation

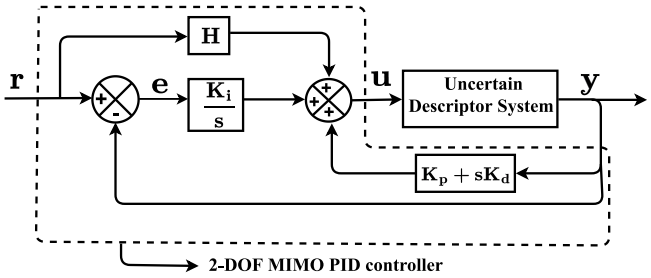

Fig. 5. Feedback interconnection of the proposed controller and uncertain plant.

capability (Anderson and Moore, 2007). The wave filter, on the other hand, helps to directly attenuate the WF disturbance, as already stated. Now, (8) can be rewritten as

$$\begin{bmatrix} I & 0\\ 0 & M\end{bmatrix}\begin{bmatrix}\dot{\eta}\\ \dot{\upsilon}\end{bmatrix} = \begin{bmatrix}0 & I\\ 0 & -D\end{bmatrix}\begin{bmatrix}\eta\\ \upsilon\end{bmatrix} + \begin{bmatrix}0\\ I\end{bmatrix}\tau,\ y = \begin{bmatrix} I & 0\end{bmatrix}\begin{bmatrix}\eta\\ \upsilon\end{bmatrix}$$

which can be represented in generalized or descriptor state-space form as

$$E\dot{x} = Ax + Bu,\ y = Cx \tag{9}$$

where

$$x = \begin{bmatrix}\eta\\ \upsilon\end{bmatrix},\ u = \tau, E = \begin{bmatrix} I & 0\\ 0 & M\end{bmatrix}, A = \begin{bmatrix}0 & I\\ 0 & -D\end{bmatrix}, B = \begin{bmatrix}0\\ I\end{bmatrix}, C = \begin{bmatrix}I\\ 0\end{bmatrix}^T.$$

In practice, the uncertainties in the hydrodynamic parameters exist in M and D matrices; therefore in (9), E and A matrices become uncertain. Note, if one expresses (9) into a standard state-space description, i.e., $\dot{x} = E^{-1}Ax + E^{-1}Bu$, then it is difficult to handle uncertainties in E and A matrices both, because in that case, the overall uncertainty occurs in nonlinear (product) form.

3.2. Uncertainty representation

Let, $M = M_0 + \Delta M,\ D = D_0 + \Delta D$ where, $M_0,\ D_0$ are the nominal values and $\Delta M,\ \Delta D$ are norm-bounded time-varying perturbations. Suppose, $\Delta M,\ \Delta D$ are represented as

$$\Delta M = ZF(t)N_M,\ \Delta D = ZF(t)N_D \tag{10}$$

with $F^T(t)F(t) < I$. Consequently, the state-space matrices of the uncertain system (9) become

$$E = E_0 + \bar{Z}F(t)\bar{N}_M,\ A = A_0 + \bar{Z}F(t)\bar{N}_D \tag{11}$$

where,

$$\begin{aligned}&E_0 = \begin{bmatrix} I & 0\\ 0 & M_0\end{bmatrix},\ A_0 = \begin{bmatrix}0 & I\\ 0 & -D_0\end{bmatrix},\ \bar{Z} = \begin{bmatrix}0\\ Z\end{bmatrix},\\ &\bar{N}_M = \begin{bmatrix}0 & N_M\end{bmatrix},\ \bar{N}_D = \begin{bmatrix}0 & -N_D\end{bmatrix}.\end{aligned} \tag{12}$$

Note, the uncertainty structure used in (10) represents a class of matched uncertainties, which is widely used in norm-bounded uncertain system literature (Khargonekar et al., 1990; Xie, 1996; Ren and Zhang, 2010). The design method to be presented can also be extended for different $Z, F(t)$ in ΔM and ΔD, but in that case, the results may be conservative.

3.3. Proposed 2-DOF MIMO PID control design

For the plant (9) with uncertain matrices of the form (11), the 2-DOF MIMO PID controller to be used is shown in Fig. 5. The control law can be written as

$$u = K_p y + K_d\frac{dy}{dt} + K_i\int_0^t (r - y)dt + Hr. \tag{13}$$

Here, the PD part is kept in the feedback channel to reduce the effect of derivative and proportional kicks on output and control input, which occur when a step reference input is applied (Ang et al., 2005). The feedforward gain H is introduced to get better tracking performance. The controller is designed in two stages: In stage 1, the feedback parameters, i.e., K_p, K_i, K_d are obtained to meet some LQ performance even in presence of parameter variations. The feedforward gain H is designed in stage 2 to further improve the r-to-y behavior. To reduce the effect of measurement noise and to make the controller causal, a low pass filter is employed in cascade with the derivative gain K_d. This derivative filter is given by

$$F_D(s) = \frac{1}{\tau_d s + 1} I_3 \tag{14}$$

where, τ_d is filter time constant and I_3 is 3×3 identity matrix. One chooses $\tau_d \ll \|K_d\|_2/\|K_p\|_2$, so that it not only retains the closed-loop stability but also does not affect the behavior of ideal PID control much (Skogestad and Postlethwaite, 2009; Ang et al., 2005; Pradhan and Ghosh, 2015).

3.4. Design of feedback parameters K_p, K_i, K_d

Below, the design of gains K_p, K_i, K_d is carried out via state feedback control of an augmented system as described below.

3.4.1. The state feedback-based transformation of the PID control law with $H = 0$

Lemma 1. *The design of PID control law (13) with $H = 0$ for the plant (9) with uncertainties as in (11), (12), is equivalent to designing a state feedback control law*

$$u = \bar{K}\bar{x},\ \bar{K} = \begin{bmatrix} K_p & K_d & K_i \end{bmatrix} \tag{15}$$

for the augmented uncertain descriptor system

$$\bar{E}\dot{\bar{x}} = \bar{A}\bar{x} + \bar{B}u + \bar{G}r,\ y = \bar{C}\bar{x} \tag{16}$$

where

$$\bar{E} = \bar{E}_0 + \bar{M}F(t)N_e,\ \bar{A} = \bar{A}_0 + \bar{M}F(t)N_a,\ \bar{B} = \begin{bmatrix} B \\ 0 \end{bmatrix},\ \bar{G} = \begin{bmatrix} 0 \\ I \end{bmatrix},$$
$$\bar{C} = [C \quad 0],\ \bar{E}_0 = \begin{bmatrix} E_0 & 0 \\ 0 & I \end{bmatrix},\ \bar{A}_0 = \begin{bmatrix} A_0 & 0 \\ -C & 0 \end{bmatrix},\ \bar{M} = \begin{bmatrix} \bar{Z} \\ 0 \end{bmatrix},$$
$$N_e = \begin{bmatrix} \bar{N}_M & 0 \end{bmatrix},\ N_a = \begin{bmatrix} \bar{N}_D & 0 \end{bmatrix}. \tag{17}$$

Proof. With $H = 0$, the PID control law in (13) can be represented as

$$u = K_p y + K_d \frac{dy}{dt} + K_i \int_0^t (r - y)dt. \tag{18}$$

Now, suppose $\xi = \int_0^t (r - y)dt$. As $y = \eta$ and $\dot{y} = \dot{\eta} = v$, the above control law can be rewritten as

$$u = \bar{K}[\eta^T \quad v^T \quad \xi^T]^T \tag{19}$$

which can be represented as (15) with

$$\bar{x} = [x^T \quad \xi^T]^T = [\eta^T \quad v^T \quad \xi^T]^T. \tag{20}$$

Augmenting the state ξ to the uncertain system (9), the augmented uncertain system corresponding to the state feedback law (19) becomes

$$\begin{bmatrix} E & 0 \\ 0 & I \end{bmatrix} \begin{bmatrix} \dot{x} \\ \dot{\xi} \end{bmatrix} = \begin{bmatrix} A & 0 \\ -C & 0 \end{bmatrix} \begin{bmatrix} x \\ \xi \end{bmatrix} + \begin{bmatrix} B \\ 0 \end{bmatrix} u + \begin{bmatrix} 0 \\ I \end{bmatrix} r$$

$$y = \begin{bmatrix} C & 0 \end{bmatrix} \begin{bmatrix} x \\ \xi \end{bmatrix}$$

which can be represented as (16) where the system matrices become same as given in (17). □

In view of the above result, we only need to design the state feedback control law (15) for the augmented uncertain descriptor system (16) to achieve robust LQ performance. The following well known LMI results will be used in this context.

A. *Schur's complement (Boyd et al., 1994):* The LMI

$$\begin{bmatrix} Q & S \\ S^T & R \end{bmatrix} > 0 \tag{21}$$

with $Q = Q^T$, $R = R^T$ is equivalent to the matrix inequalities

$$R > 0,\ Q - SR^{-1}S^T > 0. \tag{22}$$

B. *Congruence transformation (Boyd et al., 1994):* For a matrix $X = X^T$, iff $X < 0$ then $WXW^T < 0$ where W is a non-singular matrix.

We will also use the following important results.

Lemma 2 (*Petersen, 1987; Ren and Zhang, 2010*). *Given matrices $H = H^T$, U, V of appropriate dimensions, the matrix inequality*

$$H + UF(t)V + [UF(t)V]^T < 0$$

holds for all $F(t)$ satisfying $F^T(t)F(t) < I$, if and only if there exists a scalar $\epsilon > 0$ such that

$$H + \epsilon UU^T + \epsilon^{-1}V^T V < 0.$$

Lemma 3. *Consider the uncertain system (16) with $\bar{E}$ of full rank, $r = 0$, $\bar{x}(0) = \bar{x}_0$. Let the pair $(\bar{E}_0^{-1}\bar{A}_0, \bar{E}_0^{-1}\bar{B})$ be stabilisable. Then, the control law $u = \bar{K}\bar{x}$ ensures quadratic stability of the closed-loop system and minimizes the performance index*

$$J = \int_0^\infty \left[\bar{x}^T Q \bar{x} + u^T R u\right] dt,\ Q = Q^T > 0,\ R = R^T > 0 \tag{23}$$

if and only if there exist matrices $X_1 = X_1^T > 0$, X_0, Y of appropriate dimensions such that following problem is solved:

$$\min_{X_1,\ X_0} \{trace(QX_1) + trace(X_0)\} \tag{24}$$

subject to the matrix inequalities

$$\bar{E}^{-1}(\bar{A}X_1 + \bar{B}Y) + (X_1\bar{A}^T + Y^T\bar{B}^T)\bar{E}^{-T} + \bar{x}_0\bar{x}_0^T < 0 \tag{25}$$

$$\begin{bmatrix} X_0 & * \\ Y^T R^{1/2} & X_1 \end{bmatrix} > 0. \tag{26}$$

Then, the state feedback gain $\bar{K}$ becomes

$$\bar{K} = YX_1^{-1}. \tag{27}$$

Proof. The result follows directly from Duan and Yu (2013) (Ch. 8, Th. 8.9). □

Next, the matrix inequality problem of Lemma 3 is expressed as an LMI problem. The derivation is based on the LMI results of Ren and Zhang (2010), where $\mathcal{H}_\infty$ cost is used in place of the LQ cost considered in this paper. It is noteworthy that if one uses weighted $\mathcal{H}_\infty$ cost as in Ren and Zhang (2010), then the dynamic weights will increase the order of the system and as a result, the PID control law cannot be transformed into a direct state feedback control problem as in Lemma 1.

Theorem 1. *The matrix inequality problem given by (24)–(26) is solvable if and only if there exist a scalar $\epsilon > 0$, matrices $X_1 = X_1^T > 0$, X_0, X_2, X_3 and Y of appropriate sizes such that the following LMI problem is solved:*

$$\min_{X_1,\ X_0} \{trace(QX_1) + trace(X_0)\}$$

subject to

$$\begin{bmatrix} X_2+X_2^T & * & * & * \\ L_{21} & -\bar{E}_0X_3 - X_3^T\bar{E}_0^T + \epsilon\bar{M}\bar{M}^T & * & * \\ 0 & \bar{x}_0^T\bar{E}_0^T & -I & * \\ -N_eX_2+N_aX_1 & -N_eX_3 & N_e\bar{x}_0 & -\epsilon I \end{bmatrix} < 0 \quad (28)$$

$$\begin{bmatrix} X_0 & * \\ Y^T R^{1/2} & X_1 \end{bmatrix} > 0 \quad (29)$$

where, $L_{21} = -\bar{E}_0X_2 + X_3^T + \bar{A}_0X_1 + \bar{B}Y$. *Then, the gain* $\bar{K}$ *can be found as*

$$\bar{K} = YX_1^{-1}. \quad (30)$$

Proof. In Theorem 1, the LMI (29) is same as the LMI (26) of Lemma 3. Thus, below, we prove that the matrix inequality (25) holds if and only if the LMI (28) is satisfied.

Pre- and post-multiplying (25) by $\bar{E}$ and $\bar{E}^T$, respectively, and subsequently applying congruence transformation one gets

$$(\bar{A}X_1 + \bar{B}Y)\bar{E}^T + \bar{E}(X_1\bar{A}^T + Y^T\bar{B}^T) + \bar{E}\bar{x}_0\bar{x}_0^T\bar{E}^T < 0. \quad (31)$$

Then, applying Schur's complement to (31) one obtains the matrix inequality

$$\begin{bmatrix} (\bar{A}X_1 + \bar{B}Y)\bar{E}^T + \bar{E}(X_1\bar{A}^T + Y^T\bar{B}^T) & * \\ \bar{x}_0^T\bar{E}^T & -I \end{bmatrix} < 0. \quad (32)$$

Now, one can always choose a matrix X_2 such that

$$X_2 + X_2^T < 0 \quad (33)$$

and (32) is satisfied. Consequently, (32), (33) together is equivalent to the matrix inequality

$$\begin{bmatrix} X_2+X_2^T & * & * \\ 0 & (\bar{A}X_1 + \bar{B}Y)\bar{E}^T + \bar{E}(X_1\bar{A}^T + Y^T\bar{B}^T) & * \\ 0 & \bar{x}_0^T\bar{E}^T & -I \end{bmatrix} < 0. \quad (34)$$

Let

$$X_3 = -X_1\bar{A}^T - Y^T\bar{B}^T - X_2\bar{E}^T. \quad (35)$$

Then (34) becomes

$$\begin{bmatrix} X_2+X_2^T & * & * \\ X_3^T + \bar{A}X_1 + \bar{B}Y + \bar{E}X_2^T & L_{22} & * \\ 0 & \bar{x}_0^T\bar{E}^T & -I \end{bmatrix} < 0 \quad (36)$$

where, $L_{22} = \bar{A}X_1\bar{E}^T + \bar{B}Y\bar{E}^T + \bar{E}X_1\bar{A}^T + \bar{E}Y^T\bar{B}^T$. As X_3 is a free variable, (36) can always be satisfied if (34) holds. On the other hand, if (34) holds, then (32) is also satisfied. This implies that (36) is a necessary condition for (32) to hold. Now, if (36) holds then (32) also holds, since the left hand-side (LHS) of (32) is the lower (2×2) block-diagonal element of LHS of (36). Hence, (36) is a necessary and sufficient condition for (32) to hold. Next, it is shown that (36) is satisfied if and only if (28) holds. To this end, pre- and post-multiplying (36) by the matrix

$$W = \begin{bmatrix} I & 0 & 0 \\ -\bar{E} & I & 0 \\ 0 & 0 & I \end{bmatrix} \quad (37)$$

and W^T, respectively, and subsequently applying the congruence transformation, one obtains the matrix inequality

$$\begin{bmatrix} X_2+X_2^T & * & * \\ -\bar{E}X_2 + X_3^T + \bar{A}X_1 + \bar{B}Y & -\bar{E}X_3 - X_3^T\bar{E}^T & * \\ 0 & \bar{x}_0^T\bar{E}^T & -I \end{bmatrix} < 0. \quad (38)$$

Now, (38) can be rearranged to get the matrix inequality

$$\begin{bmatrix} X_2+X_2^T & * & * \\ -\bar{E}_0X_2 + X_3^T + \bar{A}_0X_1 + \bar{B}Y & -\bar{E}_0X_3 - X_3^T\bar{E}_0^T & * \\ 0 & \bar{x}_0^T\bar{E}_0^T & -I \end{bmatrix} +$$

$$\mathrm{Sym}\left\{ \begin{bmatrix} 0 & \bar{M}^T & 0 \end{bmatrix}^T F(t) \begin{bmatrix} -N_eX_2+N_aX_1 & -N_eX_3 & N_e\bar{x}_0 \end{bmatrix} \right\} < 0. \quad (39)$$

Then, following Lemma 2, (39) holds for $F^T(t)F(t) < I$, if and only if there exists a scalar $\epsilon > 0$ such that the following matrix inequality holds:

$$\begin{bmatrix} X_2+X_2^T & * & * \\ -\bar{E}_0X_2 + X_3^T + \bar{A}_0X_1 + \bar{B}Y & -\bar{E}_0X_3 - X_3^T\bar{E}_0^T + \epsilon\bar{M}\bar{M}^T & * \\ 0 & \bar{x}_0^T\bar{E}_0^T & -I \end{bmatrix}$$

$$+ \epsilon^{-1}\begin{bmatrix} (-N_eX_2+N_aX_1)^T \\ (-N_eX_3)^T \\ (N_e\bar{x}_0)^T \end{bmatrix}\begin{bmatrix} -N_eX_2+N_aX_1 & -N_eX_3 & N_e\bar{x}_0 \end{bmatrix} < 0. \quad (40)$$

Next, applying Schur's complement on (40), one gets (28). □

3.4.2. Design of the feedforward gain H

Once the feedback parameter vector $\bar{K} = [K_p \quad K_d \quad K_i]$ is known, the feedforward gain H can be designed to ensure good tracking performance in $\mathcal{H}_\infty$ sense. To this end, we take the exogenous signal as $w = r$, and the regulated variable as $z = r - y$. Then, the closed-loop system becomes

$$\bar{E}\dot{\hat{x}} = \hat{A}\bar{x} + \hat{B}w, \;\; z = \hat{C}\bar{x} + \hat{D}w \quad (41)$$

where,

$$\hat{A} = \hat{A}_0 + \bar{M}F(t)N_a, \;\; \hat{A}_0 = \bar{A}_0 + \bar{B}\bar{K}, \;\; \hat{B} = \bar{G} + \bar{B}H, \;\; \hat{C} = -\bar{C}, \;\; \hat{D} = I. \quad (42)$$

Here, the objective is to find an appropriate H such that $\|z\|_2 < \gamma\|w\|_2$ for a given γ (i.e., the $\mathcal{H}_\infty$ gain of the transfer relation from w-to-z is less than γ). In this regard, we claim the following result.

Theorem 2. *The closed-loop uncertain system (41), with the gain* $\bar{K}$ *as in Theorem 1, satisfies* $\|z\|_2 < \gamma\|w\|_2$ *if and only if there exist a scalar* $\bar{\epsilon} > 0$, *matrices* $Z_1 = Z_1^T > 0$, Z_2, Z_3 *and* H *of appropriate dimensions such that following LMI holds*

$$\begin{bmatrix} Z_2+Z_2^T & * & * & * & * \\ Z_3^T + \hat{A}_0Z_1 - \bar{E}_0Z_2 & \bar{L}_{22} & * & * & * \\ \hat{C}Z_1 & 0 & -\gamma^2 I & * & * \\ 0 & H^T\bar{B}^T + \bar{G}^T & \hat{D}^T & -I & * \\ N_aZ_1 - N_eZ_2 & -N_eZ_3 & 0 & 0 & -\bar{\epsilon}I \end{bmatrix} < 0 \quad (43)$$

where, $\bar{L}_{22} = -Z_3^T\bar{E}_0^T - \bar{E}_0Z_3 + \bar{\epsilon}\bar{M}\bar{M}^T$.

Proof. It is easy to derive following Theorem 1 of Ren and Zhang (2010) that $\|z\|_2 < \gamma\|w\|_2$ if and only if there exist matrices $Z_1 = Z_1^T > 0$, Z_2 and Z_3 such that

$$\begin{bmatrix} Z_2+Z_2^T & * & * & * \\ Z_3^T + \hat{A}Z_1 - \bar{E}Z_2 & -Z_3^T\bar{E}^T - \bar{E}Z_3 & * & * \\ \hat{C}Z_1 & 0 & -\gamma^2 I & * \\ 0 & \hat{B}^T & \hat{D}^T & -I \end{bmatrix} < 0. \quad (44)$$

Now, substituting (42) in (44) and rearranging one gets the matrix inequality

$$\begin{bmatrix} Z_2+Z_2^T & * & * & * \\ Z_3^T + \hat{A}_0Z_1 - \bar{E}_0Z_2 & -Z_3^T\bar{E}_0^T - \bar{E}_0Z_3 & * & * \\ \hat{C}Z_1 & 0 & -\gamma^2 I & * \\ 0 & H^T\bar{B}^T + \bar{G}^T & \hat{D}^T & -I \end{bmatrix}$$

$$+ \mathrm{Sym}\left\{ \begin{bmatrix} 0 \\ \bar{M} \\ 0 \\ 0 \end{bmatrix} F(t) \begin{bmatrix} (-N_eZ_2 + N_aZ_1) & -N_eZ_3 & 0 & 0 \end{bmatrix} \right\} < 0. \quad (45)$$

Then, using Lemma 2 and Schur's complement in sequence as done towards the end of the proof of Theorem 1, one can show that (45) holds for $F^T(t)F(t) < I$, iff there exists a scalar $\bar{\epsilon} > 0$ such that the LMI (43) holds. □

3.5. Design of wave filter

If WF part of the motion is compensated by the controller, then it would cause unnecessary wear and tear of the actuator. So, it is important to filter out the WF component of the measurements before reaching to the controller. A notch filter is employed in each channel for this purpose (Hu and Du, 2018; Fossen, 2011). The transfer function of the notch filter is considered as

$$h_{l_i}(s) = \frac{s^2 + 2\xi\omega_n s + \omega_n^2}{(s+\omega_n)^2},\ i = 1,2,3 \tag{46}$$

where $0 < \xi < 1$ is a design parameter used to control the magnitude of notch, while the notch frequency ω_n is chosen equal to the peak frequency of the WF disturbance spectrum (Hu and Du, 2018). As this peak frequency is 1 rad/s (see Section 2.3.2), in this paper, we consider $\omega_n = 1$ rad/s. Further, we choose $\xi = 0.1$ with which, the notch filter provides gain attenuation of around 20 dB at the notch frequency of 1 rad/s. On the other hand, at least 20 dB gain attenuation at this frequency is expected to be provided by the cascade combination of the plant and the controller. Thus, the overall 40 dB gain attenuation at frequency 1 rad/s can be had to attenuate the WF motion at the output.

Although the notch frequency is much higher than the gain-crossover frequency of the feedback loop, below we present a method to guarantee closed-loop stability in presence of the notch filter. With $h_{l_i}(s)$'s in the feedback loop, the modified plant transfer function as seen by the controller $C(s)$ (i.e., PID along with derivative filter) is

$$P(s) = G(s)\text{diag}\{h_{l_i}(s)\} \tag{47}$$

where $G(s)$ is the plant transfer function along with the actuator dynamics and $h_{l_i}(s)$ is same for all three channels. The above $P(s)$ can be represented as multiplicative input type uncertain system (Skogestad and Postlethwaite, 2009) given by

$$P(s) = G(s)[I + \Delta(s)] \tag{48}$$

where $\Delta(s) = \text{diag}\{h_{l_i}(s)\} - I$. As $\Delta(s)$ is stable, using small-gain theorem (Skogestad and Postlethwaite, 2009), the closed-loop negative feedback system consisting of $P(s)$ and $C(s)$ is stable if

$$\sigma_{max}[T_0(j\omega)] < \sigma_{min}[\Delta^{-1}(j\omega)]\ \forall\ \omega \tag{49}$$

where $T_0(s) = C(s)G(s)[1 + C(s)G(s)]^{-1}$ (Skogestad and Postlethwaite, 2009). For the proposed design, this condition is verified in Section 4.2.

4. Simulation results

Here we take 3-DOF horizontal model of the supply ship Northern Clipper available in Soman et al. (2018), Alme (2008), Du et al. (2016), Hu et al. (2017), Li et al. (2020), Lin et al. (2018), Hu et al. (2015) and Fossen and Strand (1999). We consider ±20 % variation in the nominal values of the model parameters M, D. For this uncertain ship model, we design the proposed multivariable PID controller. The steps are as follows: First, the nonlinear system is linearized around the operating point at origin and expressed as descriptor system with norm-bounded uncertainties as in (9), (10), (11). Then suitable LQR weights for the cost function (23) corresponding to the augmented generalized plant (16), (17) are chosen. Next, the PID feedback gains are designed following Theorem 1 and the feedforward gain following Theorem 2. Finally, suitable derivative filter and the notch filter are chosen following (14) and (46), respectively.

For performance comparison, we also design PID controllers following (Soman et al., 2018; Martin and Katebi, 2005; Du et al., 2016). In Soman et al. (2018), a 2-DOF PID controller is designed to achieve LQ performance for the nominal vessel model only. Therein, also, the controller design is transformed into state feedback control, but without representing the system in a descriptor form, since it is assumed that the parameters of the system are fixed. The method of Martin and Katebi (2005) used for PID design of the nominal vessel model is a combined one, which brings together the advantages of the well known Davison method (Davison, 1976), Penttinen–Koivo method (Penttinen and Koivo, 1980), and Maciejowski method (Maciejowski, 1989). Therein, the PID control gains are computed as

$$K_p = pG^{-1}(j\omega_b),\ K_i = \epsilon G^{-1}(0),\ K_d = \delta(CB)^{-1} \tag{50}$$

where, ω_b is the desired closed-loop bandwidth, and p, ϵ, δ are scalar tuning parameters to be chosen suitably to achieve a desired speed of response. In above, to obtain a real approximation of $G^{-1}(j\omega_b)$, 'align' algorithm (Maciejowski, 1989; Skogestad and Postlethwaite, 2009) of MATLAB is used in Martin and Katebi (2005). Further, we compared the results with the multi-loop (or, decentralized) PID controller used in Du et al. (2016) for the same system.

Table 1
Magnitude and rate saturation limits on control forces/moments per channel.

Channel	Magnitude limit	Rate limit
Surge	3.7681×10^5 N	5.3831×10^4 N/s
Sway	6.8072×10^5 N	9.7246×10^4 N/s
Yaw	7.3119×10^6 N m	1.0446×10^6 N m/s

4.1. System parameters

The nominal values of the mass matrix and the damping matrix are:

$$M_0 = 10^9 \begin{bmatrix} 0.0053 & 0 & 0 \\ 0 & 0.0083 & 0 \\ 0 & 0 & 3.7454 \end{bmatrix},$$

$$D_0 = \begin{bmatrix} 5.0242 \times 10^4 & 0 & 0 \\ 0 & 2.7229 \times 10^5 & -4.3933 \times 10^6 \\ 0 & -4.3933 \times 10^6 & 41.8940 \times 10^7 \end{bmatrix}.$$

To tackle ±20% uncertainties in the M_0, D_0, we take $\Delta M, \Delta D$ as in (10) with

$$Z = I_3,\ N_M = 0.2M_0,\ N_D = 0.2D_0. \tag{51}$$

As mentioned in Witkowska and Śmierzchalski (2018), we consider six actuators (i.e., $q = 6$) – two main propellers in port and starboard, two tunnel thrusters in the aft, one tunnel thruster and one rotatable azimuth thruster in the bow, as shown in Fig. 6. The actuator time constant matrix is considered as

$$T_a = 7I_6 \tag{52}$$

where, I_6 is 6×6 identity matrix. In above, although each actuator is considered to have equal time constant (i.e., 7 s), it does not matter if they differ, as long as the same is much less than closed-loop system time constant. We assume the thrust angle of the azimuth thruster to be 90° (Witkowska and Śmierzchalski, 2018), to obtain the actuator configuration matrix as

$$B_{\bar{u}} = \begin{bmatrix} 1 & 1 & 0 & 0 & 0 & 0 \\ 0 & 0 & 1 & 1 & 1 & 1 \\ 0.047 & -0.047 & -0.411 & -0.386 & 0.455 & 0.337 \end{bmatrix}.$$

A real vessel has actuator saturation limits that restrict the control input. In order to incorporate such effects, the control performance is tested with the saturation limits on maximum control forces/moments and rate of change in control forces/moments per channel. These limits are selected by assuming a maximum speed of 7.5 m/s in surge, 2.5 m/s in sway and 60 degree/min. in yaw directions (Alme, 2008) (Ch. 5). The actuator limits used are shown in Table 1.

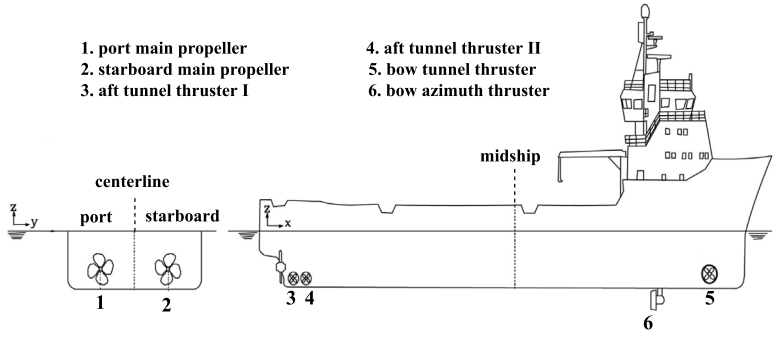

Fig. 6. Locations of thrusters and propellers on the supply vessel (Ahani and Ketabdari, 2019).

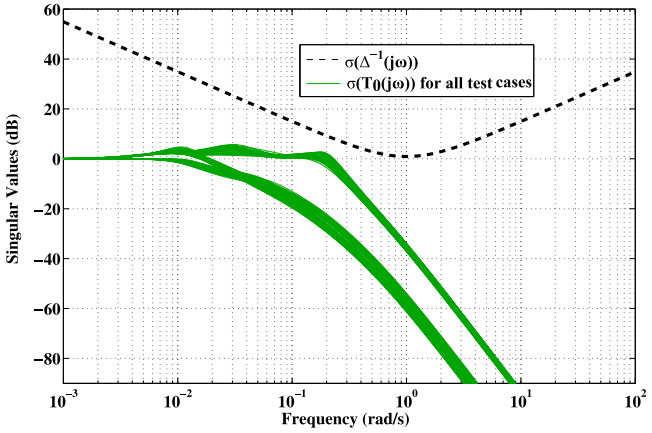

Fig. 7. Singular value plots of Δ^{-1} and T_0's for 50 random plants within the uncertainly set.

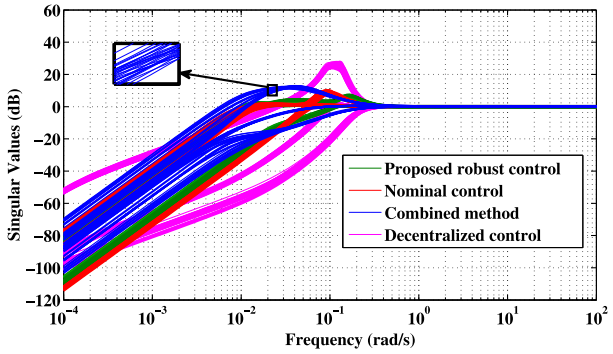

Fig. 8. Singular value plots of S's corresponding to 50 random plants within the uncertainty set. (Nominal control: Soman et al. (2018); Combined method: Martin and Katebi (2005); Decentralized control: Du et al. (2016)).

4.2. Controller parameters

To design PID controller, the LQR weights are chosen as $Q = \text{diag}\{5\times10^5, 8\times10^7, 8\times10^7, 10^5, 10^7, 10^7, 300, 10^5, 3\times10^8\}$, $R = \text{diag}\{4, 0.03, 0.06\}$. Here, for convenience, diagonal LQR weights are chosen. As the surge channel is decoupled from the other two channels and is comparatively faster, lesser weights are given on the states corresponding to the surge channel [i.e., $Q(1,1), Q(4,4), Q(7,7)$]. To handle the strong coupling between sway and yaw channels, more weights are given on the states corresponding to sway [i.e., $Q(2,2), Q(5,5), Q(8,8)$] and yaw channels [i.e., $Q(3,3), Q(6,6), Q(9,9)$]. In the control weight R, a lesser weight is given on the inputs corresponding to the sway and yaw channels [i.e., $R(2,2), R(3,3)$], so that control input can increase more freely to reduce the coupling effect. With these settings, the PID gains are obtained following Theorem 1 as

$$K_p = \begin{bmatrix} -1.2792\times10^3 & 0 & 0 \\ 0 & -4.9223\times10^4 & 1.5976\times10^6 \\ 0 & 3.9852\times10^4 & -6.2542\times10^6 \end{bmatrix},$$

$$K_d = \begin{bmatrix} -7.2727\times10^4 & 0 & 0 \\ 0 & -1.7626\times10^6 & 8.3428\times10^7 \\ 0 & -1.3969\times10^5 & -7.0376\times10^7 \end{bmatrix},$$

$$K_i = \begin{bmatrix} 6.9094 & 0 & 0 \\ 0 & 4.9101\times10^2 & -8.3197\times10^2 \\ 0 & -1.4403\times10^2 & 3.8242\times10^4 \end{bmatrix}.$$

As $\|K_d\|_2/\|K_p\|_2 = 16.90$, we choose the derivative filter time constant $\tau_d = 1.69$ s. Further following Theorem 2, the feedforward gain (corresponding to the minimised γ) is obtained as

$$H = \begin{bmatrix} 0.1129\times10^3 & 0 & 0 \\ 0 & -0.1429\times10^4 & -0.8423\times10^4 \\ 0 & -0.0392\times10^3 & -0.2933\times10^4 \end{bmatrix}.$$

Next, with the above controller gains, following the results in Section 3.5, we test if the closed-loop system with notch filter remains stable. The singular value plots of $T_0(s)$'s corresponding 50 randomly chosen $G(s)$'s from the uncertainty set given in Section 4.1, are shown in Fig. 7, The singular value plot of $\Delta^{-1}(s)$ is also shown in this figure. From the figure, it is clear that the condition (49) is satisfied, implying the closed-loop system stability is guaranteed with the notch filter.

4.3. Frequency response

To study the robustness of the uncertain compensated system using frequency response, we consider sensitivity function $S(s)$, complementary sensitivity function $T(s)$, and control sensitivity function $S(s)K(s)$, where $S(s) = [I + L(s)]^{-1}$, $T(s) = L(s)[I + L(s)]^{-1}$, $L(s) = K(s)G(s)$ with $G(s)$ being the uncertain plant including the actuator dynamics and $K(s)$ the PID controller including the derivative and notch filters (in a negative feedback loop). It is well known that, $\|S\|_\infty, \|T\|_\infty, \|SK\|_\infty$ are the measures of robustness against parametric uncertainties and different unmodeled dynamics. In addition, $\|SK\|_\infty$ is the measure of maximum control input magnitude (Skogestad and Postlethwaite, 2009).

To check if all the above margins are satisfactory with the proposed design even in presence of parametric uncertainty, we take 50 randomly chosen plants within the specified uncertainties limit. For all these sample plants, the proposed as well as existing PID controllers (Martin and

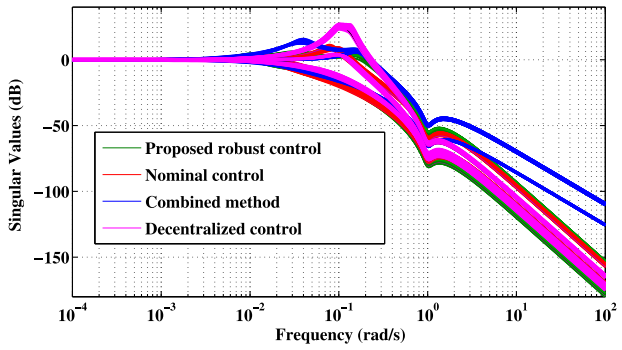

Fig. 9. Singular value plots of T's corresponding to 50 random plants within the uncertainty set.

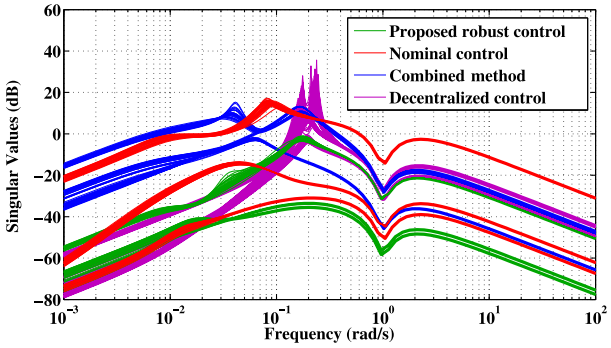

Fig. 10. Singular value plot of SK's corresponding to 50 random plants within the uncertainty set.

Katebi, 2005; Soman et al., 2018; Du et al., 2016) have been employed. The singular value plots are shown in Figs. 8, 9, 10. Table 2 shows that, with the existing controllers (Soman et al., 2018; Martin and Katebi, 2005; Du et al., 2016), the worst (i.e., maximum corresponding to all sample plants) values of $\|S\|_\infty$ and $\|T\|_\infty$ are much higher than the safe limit of 2 (i.e., 6 dB) (Skogestad and Postlethwaite, 2009), whereas with the proposed control, these are very near to 2. The extremely large values of $\|S\|_\infty$ and $\|T\|_\infty$ with the decentralized PID control may even lead to instability in presence of uncertainties. Further, Table 2 shows that with the proposed control, the worst value of $\|SK\|_\infty$ is less than 1, whereas with the other three methods the same is much higher than 1. This implies that with the existing PIDs, the control efforts are expected to be more as compared to the proposed one. The pathological situation happens with decentralized PID control, as expected.

Further, to study the LF and WF disturbance attenuation behavior with the proposed control, the transfer functions from w_d-to-y, i.e., GS and from v_d-to-y, i.e., $-GSK$ are considered. The singular value plots of these two transfer functions with all four approaches are shown in Figs. 11, 12. Fig. 11 shows that in the absence of constraints on control effort, the LF attenuation behavior with all four designs are quite good (less than −50 dB). On the other hand, Fig. 12 shows that under no actuator constraints, at the wave frequency, the WF disturbance gets attenuated with the proposed method at least by a factor of 400, whereas the same for nominal LQ method, combined method, and decentralized control method, respectively, are 179, 127 and 89. It is inferred that the above improvements with the proposed control would become more prominent in presence of constraints on control effort, because the control efforts with the existing three designs are much more as compared to the proposed design, as already discussed towards the end of second paragraph above.

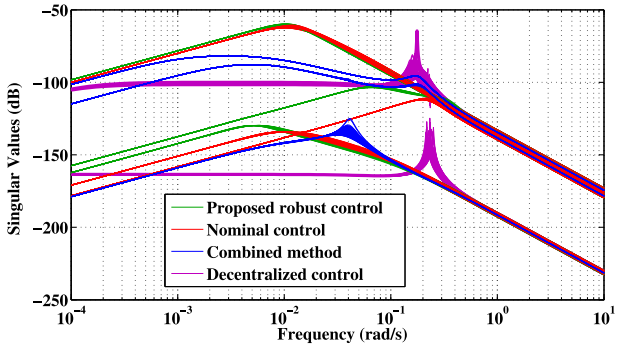

Fig. 11. Singular value plot of GS's corresponding to 50 random plants within the uncertainty set.

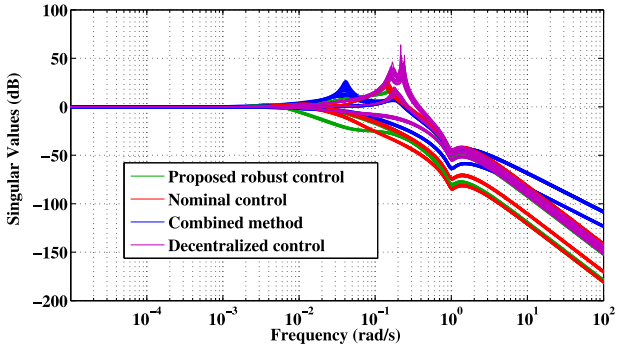

Fig. 12. Singular value plot of GSK's corresponding to 50 random plants within the uncertainty set.

Table 2
Worst-case robustness margins for the perturbed plants.

PID control method	$\|S\|_\infty$	$\|T\|_\infty$	$\|SK\|_\infty$
Proposed robust LQ control	2.03	2.09	0.89
Nominal LQ control (Soman et al., 2018)	2.57	2.66	7.07
Combined method (Martin and Katebi, 2005)	3.98	5.62	5.95
Decentralized control (Du et al., 2016)	25.11	22.38	63.09

4.4. Time-response

To study the time-response with the proposed as well as existing PID controllers (Martin and Katebi, 2005; Soman et al., 2018; Du et al., 2016), we considered the parameters of the system as given in Section 4.1 with +20% variation in M matrix and −20% variation in D matrix. Note, this is the worst-case scenario in the considered uncertainty set. For simulation purpose, we consider the system of Fig. 4 with the uncertainties in the ship dynamics as above. Saturation blocks at the inputs (τ) with the magnitude and rate limits, as given in Table 1, are also included in the simulation. All the simulations are carried out in MATLAB–Simulink. The relevant results obtained are presented next.

4.4.1. Response in station keeping

In station keeping, the ship is required to maintain its position and course even in presence of LF and WF disturbances, such as wind, wave and ocean currents, as discussed in Sections 2.3.1, 2.3.2. The closed-loop responses of the considered perturbed plant in presence of these disturbances are shown in Fig. 13. Note, it is verified that the closed-loop perturbed system with the decentralized PID control (Du et al., 2016) becomes unstable, as inferred from the frequency response studies in Section 4.3 as well. Fig. 13 shows that the proposed controller achieves much superior WF disturbance attenuation in presence of

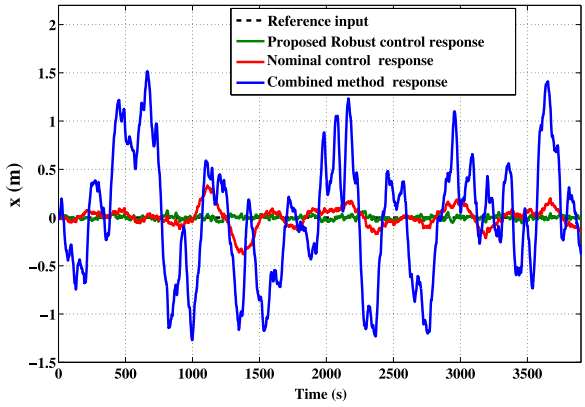

(a) Surge channel.

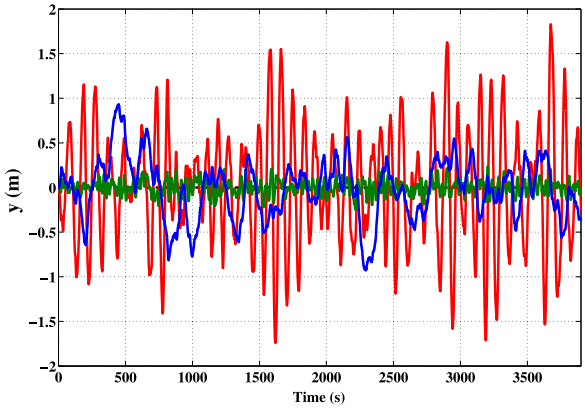

(b) Sway channel.

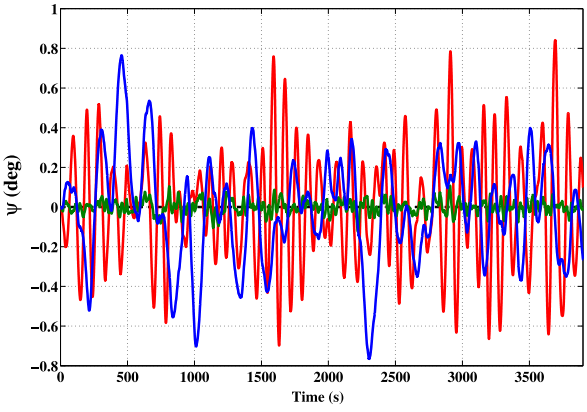

(c) Yaw channel.

Fig. 13. Closed-loop response of uncertain system in station keeping (Nominal control: Soman et al. (2018); Combined method: Martin and Katebi (2005)).

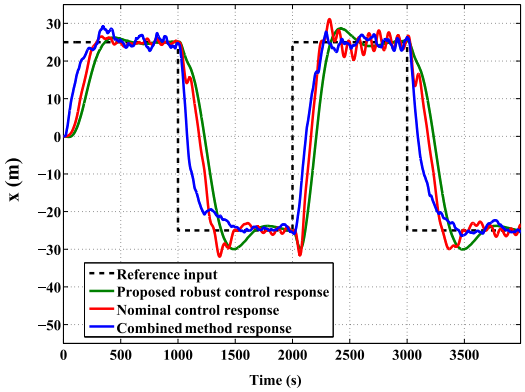

(a) Surge channel.

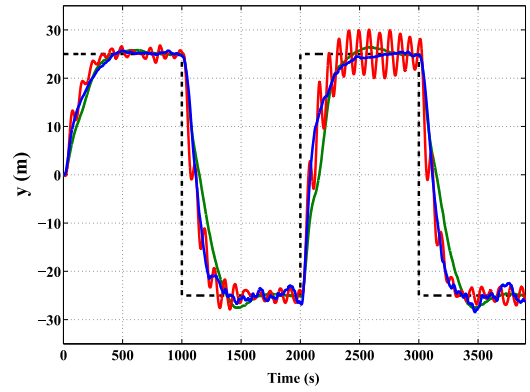

(b) Sway channel.

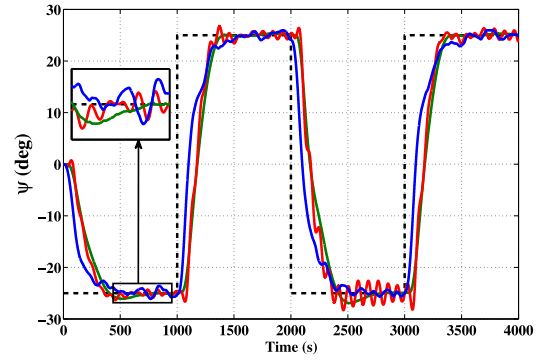

(c) Yaw channel.

Fig. 14. Closed-loop response of uncertain system in low speed maneuvering.

uncertainties in the system parameters and the actuator constraints, as expected. On the other hand, the disturbance attenuation with the existing controllers (Soman et al., 2018; Martin and Katebi, 2005) is poor because, the uncertainties in the system parameters are not considered explicitly in the designs, unlike in the proposed approach.

4.4.2. Response in low speed maneuvering

To study the performance of the proposed controller along with the existing ones in low speed maneuvering, the following worst directions of square wave reference inputs are applied:

(i) ±25 m in surge direction
(ii) ±25 m in sway direction
(iii) ∓25 degree in yaw direction.

Table 3
Comparison of time-domain performance.

Performance index	Nominal response (surge, sway, yaw)			Perturbed response (surge, sway, yaw)		
	Proposed robust control	Nominal control (Soman et al., 2018)	Combined method (Martin and Katebi, 2005)	Proposed robust control	Nominal control (Soman et al., 2018)	Combined method (Martin and Katebi, 2005)
IAE (m s, m s, deg s)	5930, 4421, 9.36×10^4	5699, 5102, 9.48×10^4	6941, 4359, 9.4×10^4	5942, 4289, 9.36×10^4	6515, 6492, 9.9×10^4	7112, 4583, 9.95×10^4
ITAE (m s^2, m s^2, deg s^2)	1.13×10^6, 9.07×10^5, 9.16×10^5	3.11×10^6, 4.69×10^6, 3.13×10^6	1.00×10^7, 3.01×10^7, 1.9×10^8	1.14×10^6, 8.83×10^5, 9.18×10^5	4.71×10^6, 7.73×10^6, 4.27×10^6	1.06×10^7, 3.37×10^7, 1.96×10^8
Rise time (s)	194.31, 261.45, 227.77	160.67, 220.02, 198.11	148.84, 256.03, 233.20	189.50, 255.05, 240.80	143.41, 194.07, 193.78	137.40, 237.89, 252.25
Max. overshoot (%)	4.7, 4.37, 1.99	5.55, 4.81, 3.23	6.45, 2.57, 2.69	4.73, 3.64, 1.99	7.06, 8.50, 3.16	7.13, 2.69, 4.23
Max. undershoot (%)	2.04, 1.99, 4.15	1.99, 4.70, 3.75	10.98, 3.42, 5.54	2.44, 1.99, 4.53	4.91, 5.75, 4.62	11.76, 3.24, 6.06
$\|\tau_i\|_2$	5.78×10^5, 3.28×10^6, 2.06×10^7	1.33×10^6, 6.51×10^6, 2.42×10^7	4.25×10^6, 5.01×10^6, 1.8×10^7	5.80×10^5, 3.35×10^6, 2.45×10^7	1.66×10^6, 8.27×10^6, 2.65×10^7	5.06×10^6, 6.09×10^6, 2.21×10^7
$\|\dot{\tau}_i\|_2$	9.27×10^5, 5.36×10^6, 1.00×10^7	3.04×10^6, 2.11×10^7, 1.33×10^7	6.27×10^6, 7.41×10^7, 1.06×10^7	9.31×10^5, 5.41×10^6, 1.03×10^7	3.18×10^6, 3.74×10^7, 5.52×10^7	6.49×10^6, 7.81×10^7, 1.53×10^7

The above reference input magnitudes are chosen such that the compensated system operates far away from the nominal operating point (at origin). Along with the reference inputs, the considered LF and WF disturbances, as in Sections 2.3.1, 2.3.2, are also applied simultaneously. The closed-loop output responses for the uncertain nonlinear systems with all three designs are shown in Fig. 14. The corresponding force/torque magnitudes and rates are shown in Figs. 15, 16, respectively. From Fig. 14(a), (b), (c), it can be seen that surge, sway, and yaw channels have maximum speed of 0.33 m/s, 0.31 m/s and 17.19 degree/min, respectively, which are well within the respective maximum values mentioned in Section 4.1. Fig. 14 shows that the proposed control achieves desired tracking performance even in presence of LF, WF disturbances, and uncertainties in system parameters, whereas the effect of WF disturbance is very much prominent with the two existing approaches. With the proposed control, the force/torque magnitudes are also within the desired limits in all three channels. The force/torque rate, in sway channel, however, reaches to saturation value, which is true for the other two methods as well. With the nominal LQ method and the combined method, this saturation occurs even in surge and sway channels. With these two methods the control input magnitudes are also more than the proposed one in all three channels.

At the end, it is noteworthy that, although the present design guarantees robust performance behavior for ±20 % variation in M, D matrices, it is checked through simulations that the robust performance behavior retains till ±25 % variation in M and ±30 % variation in D matrices. This implies that the guaranteed tolerable uncertainty limits for robust performance are not too far from the ones obtained by post-checking, which implies that the proposed design is not too conservative.

4.5. Comparison based on some time-domain performance indices

To show the superiority of the proposed design based on some direct data comparison, the following time-domain performance indices are considered for all three channels:

- Integral absolute error (IAE) $:= \int_0^\infty |e_i|dt$
- Integral time absolute error (ITAE) $:= \int_0^\infty t|e_i|dt$
- Rise time
- Maximum overshoot
- Maximum undershoot
- 2-norm of actuator force/torque ($\|\tau_i\|_2$)
- 2-norm of actuator force/torque rate ($\|\dot{\tau}_i\|_2$).

In above, e_i is the tracking error of the ith channel, $i = 1, 2, 3$, and as is well known, the 2-norm of a signal physically means energy of the signal.

Now, to compute the above performance measures, step reference inputs of 25 m in the surge direction, 25 m in sway direction and −25 degree in yaw direction are applied simultaneously from $t = 0$ to 4000 s. The LF and WF disturbances are also applied simultaneously. The values of the above-listed performance indices computed for all three channels are presented in Table 3. It shows the following:

A. With the proposed control, IAE under nominal condition is less as compared to that with the methods of Soman et al. (2018) and Martin and Katebi (2005) for all three channels. In presence of uncertainties, with the proposed control, IAE remains close to the one under nominal condition. But with the other two methods, IAE under perturbed condition increases considerably. The same happens for ITAE performance index as well.
B. The rise time with the proposed robust design is, however, little bit more as compared to that with the other two designs. This is because, the robust performance design makes the system slow.
C. The overshoots/undershoots with the proposed design are less as compared to those with the other two designs in most cases. Also, with the proposed scheme, they remain close to the nominal values even in presence of uncertainties.
D. Under nominal case, the 2-norm of actuator torque in yaw channel is more or less same for all three designs. In other two channels, this norm value is much less with the proposed design. More importantly, with the proposed design, these norm values remain close to the nominal ones under perturbed condition as well, unlike with the other two existing designs. Same is the case for 2-norm of rate of actuator force/torque as well.

5. Conclusion

This work has designed a MIMO PID controller for DP of a ship in presence of hydrodynamic parameter uncertainties and environmental disturbances. A feedforward gain has also been introduced to the proposed PID control scheme to improve tracking performance in $\mathcal{H}_\infty$ sense. An LMI-based descriptor system approach has been proposed to design the MIMO PID controller to ensure desired LQ performance even in presence of hydrodynamic parameter uncertainties. The performance of the proposed control has been compared with the existing approaches. Simulation results show that if a controller is designed only for the nominal system, then the responses may deviate drastically from

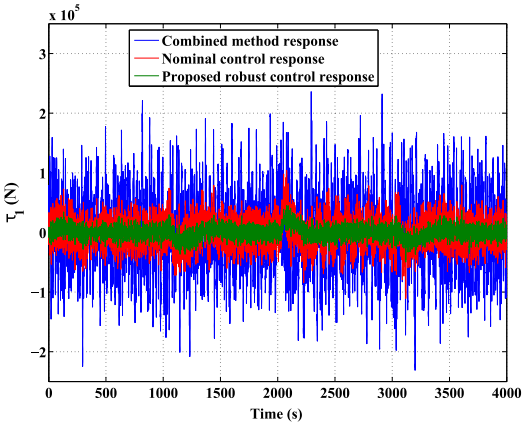

(a) Surge channel.

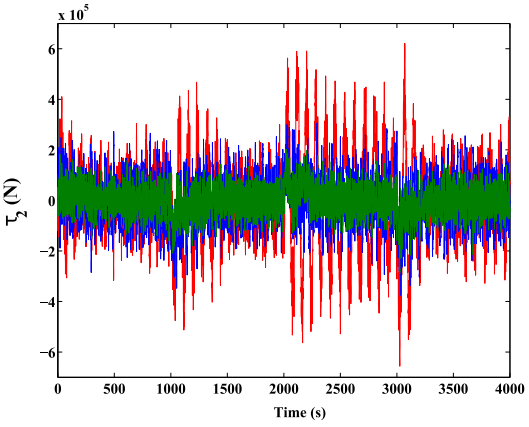

(b) Sway channel.

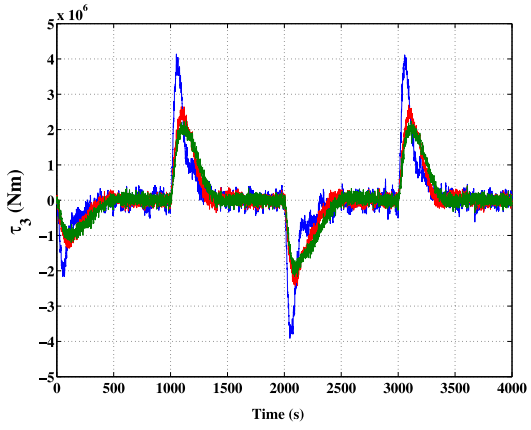

(c) Yaw channel.

Fig. 15. Control input magnitude response in low speed maneuvering.

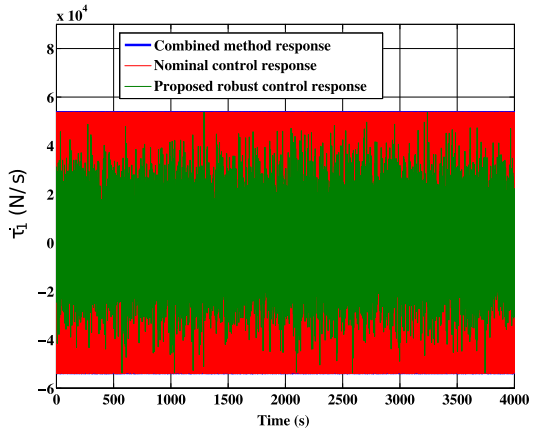

(a) Surge channel.

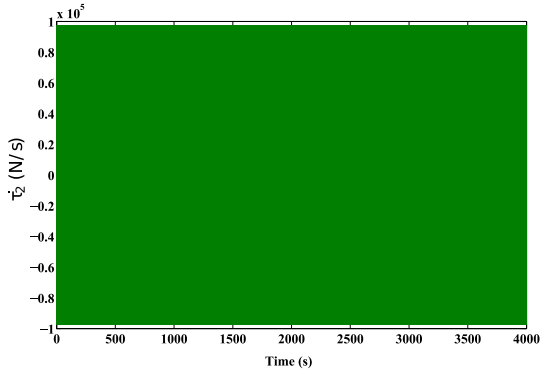

(b) Sway channel.

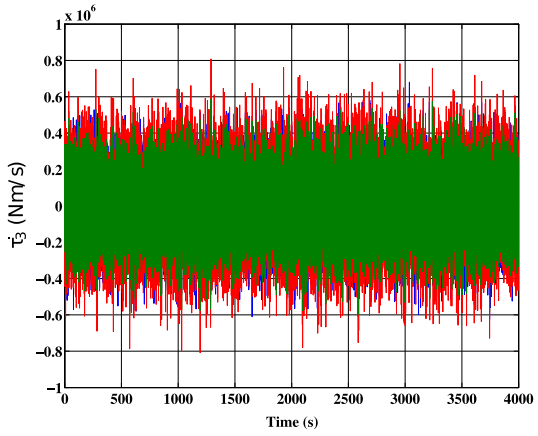

(c) Yaw channel.

Fig. 16. Control input rate response in low speed maneuvering.

the desired one if uncertainties in the hydrodynamic parameters occur in presence of actuator saturation constraints. The proposed design being based on the uncertain system, its performance is far better than the existing ones. Still in the present approach, the actuator rate saturation in sway channel is unavoidable. This is because, the actuator saturation constraints are not explicitly considered in the design process. Some LMIs to handle actuator saturation may be augmented with the proposed approach in future. The same may also be taken care of by extending the present design to include model predictive constraints in future. Another future work may be to test the efficacy of the proposed controller on an experimental prototype.

CRediT authorship contribution statement

Falguni Gopmandal: Methodology, Investigation, Writing – original draft, Writing – review & editing. **Arun Ghosh:** Conceptualization, Writing – review & editing, Supervision. **Avinash Kumar:** Investigation, Writing – original draft.

Declaration of competing interest

The authors declare that they have no known competing financial interests or personal relationships that could have appeared to influence the work reported in this paper.

Data availability

Data will be made available on request.

References

Ahani, A., Ketabdari, M.J., 2019. Alternative approach for dynamic-positioning thrust allocation using linear pseudo-inverse model. Appl. Ocean Res. 90, 101854.

Alme, J., 2008. Autotuned Dynamic Positioning for Marine Surface Vessels (M.S. Thesis). Norwegian Univ. Sci. Technol., Trondheim, Norway.

Anderson, B.D., Moore, J.B., 2007. Optimal Control: Linear Quadratic Methods. Courier Corporation.

Ang, K.H., Chong, G., Li, Y., 2005. PID control system analysis, design, and technology. IEEE Trans. Control Syst. Technol. 13 (4), 559–576.

Balchen, J.G., Jenssen, N.A., Mathisen, E., Sælid, S., 1980. A dynamic positioning system based on Kalman filtering and optimal control. Model. Identif. Control 1 (3), 135–163.

Boyd, S., El Ghaoui, L., Feron, E., Balakrishnan, V., 1994. Linear Matrix Inequalities in System and Control Theory, Vol. 15. SIAM.

Chang, W.J., Chen, G.J., Yeh, Y.L., 2002. Fuzzy control of dynamic positioning systems for ships. J. Mar. Sci. Technol. 10 (1), 47–53.

Cui, J., Yang, R., Pang, C., Zhang, Q., 2021. Observer-based adaptive robust stabilization of dynamic positioning ship with delay via Hamiltonian method. Ocean Eng. 222, 108439.

Davison, E., 1976. Multivariable tuning regulators: the feedforward and robust control of a general servomechanism problem. IEEE Trans. Automat. Control 21 (1), 35–47.

Du, J., Hu, X., Krstić, M., Sun, Y., 2016. Robust dynamic positioning of ships with disturbances under input saturation. Automatica 73, 207–214.

Du, J., Hu, X., Liu, H., Chen, C.P., 2015. Adaptive robust output feedback control for a marine dynamic positioning system based on a high-gain observer. IEEE Trans. Neural Netw. Learn. Syst. 26 (11), 2775–2786.

Duan, G.R., Yu, H.H., 2013. LMIS in Control Systems: Analysis, Design and Applications. CRC Press.

Fossen, T., 2011. Handbook of Marine Craft Hydrodynamics and Motion Control. John Wiley & Sons.

Fossen, T.I., Berge, S.P., 1997. Nonlinear vectorial backstepping design for global exponential tracking of marine vessels in the presence of actuator dynamics. In: Proceedings of the 36th IEEE Conference on Decision and Control. IEEE, pp. 4237–4242.

Fossen, T.I., Grovlen, A., 1998. Nonlinear output feedback control of dynamically positioned ships using vectorial observer backstepping. IEEE Trans. Control Syst. Technol. 6 (1), 121–128.

Fossen, T.I., Strand, J.P., 1999. Passive nonlinear observer design for ships using Lyapunov methods: full-scale experiments with a supply vessel. Automatica 35 (1), 3–16.

Hassani, V., Sørensen, A.J., Pascoal, A.M., Athans, M., 2017. Robust dynamic positioning of offshore vessels using mixed-μ synthesis modeling, design, and practice. Ocean Eng. 129, 389–400.

Hu, X., Du, J., 2018. Robust nonlinear control design for dynamic positioning of marine vessels with thruster system dynamics. Nonlinear Dynam. 94 (1), 365–376.

Hu, X., Du, J., Shi, J., 2015. Adaptive fuzzy controller design for dynamic positioning system of vessels. Appl. Ocean Res. 53, 46–53.

Hu, X., Du, J., Sun, Y., 2017. Robust adaptive control for dynamic positioning of ships. IEEE J. Ocean. Eng. 42 (4), 826–835.

Huang, Y., Wu, D., Yin, Z., Yuan, Z.M., 2021. Design of UDE-based dynamic surface control for dynamic positioning of vessels with complex disturbances and input constraints. Ocean Eng. 220, 108487.

Jayasiri, A., Nandan, A., Imtiaz, S., Spencer, D., Islam, S., Ahmed, S., 2017. Dynamic positioning of vessels using a UKF-based observer and an NMPC-based controller. IEEE Trans. Autom. Sci. Eng. 14 (4), 1778–1785.

Katebi, M., Grimble, M., Zhang, Y., 1997. H_∞ robust control design for dynamic ship positioning. IEE Proc. Control Theory Appl. 144 (2), 110–120.

Katebi, M., Yamamoto, I., Matsuura, M., Grimble, M., Hirayama, H., Okamoto, N., 2001. Robust dynamic ship positioning control system design and applications. Internat. J. Robust Nonlinear Control 11 (13), 1257–1284.

Khargonekar, P.P., Petersen, I.R., Zhou, K., 1990. Robust stabilization of uncertain linear systems: quadratic stabilizability and H_∞ theory. IEEE Trans. Automat. Control 35 (3), 356–361.

Li, J., Du, J., Hu, X., 2020. Robust adaptive prescribed performance control for dynamic positioning of ships under unknown disturbances and input constraints. Ocean Eng. 206, 107254.

Liang, K., Lin, X., Chen, Y., Li, J., Ding, F., 2020. Adaptive sliding mode output feedback control for dynamic positioning ships with input saturation. Ocean Eng. 206, 107245.

Lin, X., Nie, J., Jiao, Y., Liang, K., Li, H., 2018. Nonlinear adaptive fuzzy output-feedback controller design for dynamic positioning system of ships. Ocean Eng. 158, 186–195.

Lin, C., Wang, Q.G., Lee, T.H., 2004. An improvement on multivariable PID controller design via iterative LMI approach. Automatica 40 (3), 519–525.

Lin, C., Wang, J.L., Yang, G.H., Lam, J., 2000. Robust stabilization via state feedback for descriptor systems with uncertainties in the derivative matrix. Internat. J. Control 73 (5), 407–415.

Loueipour, M., Keshmiri, M., Danesh, M., Mojiri, M., 2015. Wave filtering and state estimation in dynamic positioning of marine vessels using position measurement. IEEE Trans. Instrum. Meas. 64 (12), 3253–3261.

Lu, J., Yu, S., Zhu, G., Zhang, Q., Chen, C., Zhang, J., 2021. Robust adaptive tracking control of UMSVs under input saturation: A single-parameter learning approach. Ocean Eng. 108791.

Maciejowski, J.M., 1989. Multivariable Feedback Design. Addison-Wesley.

Martin, P., Katebi, R., 2005. Multivariable PID tuning of dynamic ship positioning control systems. J. Mar. Eng. Technol. 4 (2), 11–24.

Penttinen, J., Koivo, H.N., 1980. Multivariable tuning regulators for unknown systems. Automatica 16 (4), 393–398.

Petersen, I.R., 1987. A stabilization algorithm for a class of uncertain linear systems. Systems Control Lett. 8 (4), 351–357.

Pradhan, J.K., Ghosh, A., 2015. Multi-input and multi-output proportional-integral-derivative controller design via linear quadratic regulator-linear matrix inequality approach. IET Control Theory Appl. 9 (14), 2140–2145.

Pradhan, J.K., Ghosh, A., 2022. Multivariable robust proportional-integral-derivative control for linear quadratic compensation of a class of norm-bounded uncertain systems. J. Dyn. Syst. Meas. Control 144 (10), 31–38.

Ren, J., Zhang, Q., 2010. Robust H_∞ control for uncertain descriptor systems by proportional–derivative state feedback. Internat. J. Control 83 (1), 89–96.

Skogestad, S., Postlethwaite, I., 2009. Multivariable Feedback Control: Analysis and Design, Vol. 2. Wiley, New York.

Soman, R.S., Gopmandal, F., Ghosh, A., 2018. MIMO PID compensation for dynamic positioning of a ship. In: Proceedings of the 5th Indian Control Conference (ICC), Kanpur, India. IEEE, pp. 137–142.

Tannuri, E., Agostinho, A., Morishita, H., Moratelli, Jr., L., 2010. Dynamic positioning systems: An experimental analysis of sliding mode control. Control Eng. Pract. 18 (10), 1121–1132.

Veksler, A., Johansen, T.A., Borrelli, F., Realfsen, B., 2016. Dynamic positioning with model predictive control. IEEE Trans. Control Syst. Technol. 24 (4), 1340–1353.

von Ellenrieder, K.D., 2019. Dynamic surface control of trajectory tracking marine vehicles with actuator magnitude and rate limits. Automatica 105, 433–442.

Wang, L., Wang, W., Du, Y., Huang, Y., 2019. A novel adaptive fuzzy PID controller based on piecewise PID controller for dynamic positioning of sandglass-type FDPSO. J. Mar. Sci. Technol. 24 (3), 720–737.

Wang, Y., Wang, H., Li, M., Wang, D., Fu, M., 2021. Adaptive fuzzy controller design for dynamic positioning ship integrating prescribed performance. Ocean Eng. 219, 107956.

Witkowska, A., Śmierzchalski, R., 2018. Adaptive dynamic control allocation for dynamic positioning of marine vessel based on backstepping method and sequential quadratic programming. Ocean Eng. 163, 570–582.

Xie, L., 1996. Output feedback H_∞ control of systems with parameter uncertainty. Internat. J. Control 63 (4), 741–750.

Xu, S., Wang, X., Yang, J., Wang, L., 2020. A fuzzy rule-based PID controller for dynamic positioning of vessels in variable environmental disturbances. J. Mar. Sci. Technol. 25 (3), 914–924.

You, S.S., Lim, T.W., Kim, J.Y., Choi, H.S., 2017. Robust control synthesis for dynamic vessel positioning. Proc. Inst. Mech. Eng. M 231 (1), 98–108.

Yu, W.Z., Xu, H.X., Feng, H., 2018. Robust adaptive fault-tolerant control of dynamic positioning vessel with position reference system faults using backstepping design. Internat. J. Robust Nonlinear Control 28 (2), 403–415.

Zhang, G., Cai, Y., Zhang, W., 2016. Robust neural control for dynamic positioning ships with the optimum-seeking guidance. IEEE Trans. Syst. Man Cybern. 47 (7), 1500–1509.

Zhang, G., Yao, M., Xu, J., Zhang, W., 2020. Robust neural event-triggered control for dynamic positioning ships with actuator faults. Ocean Eng. 207, 107292.

Zhang, D., Ye, Z., Feng, G., Li, H., 2021. Intelligent event-based fuzzy dynamic positioning control of nonlinear unmanned marine vehicles under dos attack. IEEE Trans. Cybern. http://dx.doi.org/10.1109/TCYB.2021.3128170.

Zheng, H., Wu, J., Wu, W., Zhang, Y., 2020. Robust dynamic positioning of autonomous surface vessels with tube-based model predictive control. Ocean Eng. 199, 106820.